Dental Materials 41 (2025) 451–463

Contents lists available at ScienceDirect

Dental Materials

journal homepage: www.elsevier.com/locate/dental

Development and characterization of 3D-printed denture base resin composites having self-healing potential

Mariam Raza Syed [a], Sultan Aati [a,b], Gavin Flematti [c], Jukka P. Matinlinna [d,e], Amr Fawzy [a,*]

[a] UWA Dental School, The University of Western Australia, Nedlands, WA 6009, Australia
[b] Dental Health Department, College of Applied Medical Sciences, King Saud University, Riyadh 11421, Saudi Arabia
[c] School of Molecular Sciences, The University of Western Australia, Nedlands, WA 6009, Australia
[d] Dental Materials Science, Applied and Oral Science and Community Oral Care, Faculty of Dentistry, The University of Hong Kong, Hong Kong
[e] Applied Dental Sciences, Biomaterials Science, Division of Dentistry, University of Manchester, M13 9PL, UK

ARTICLE INFO

Keywords:
Additive manufacturing
3D-printing dentures
Resin composites
Self-healing microcapsules
Fracture toughness
Dental materials

ABSTRACT

Objective: This study aims to develop and characterize 3D-printed denture resin composites containing self-healing polyurea formaldehyde (PUF) microcapsules (TEGDMA as the core healing agent) for arresting micro-cracks formation and enhancing the mechanical durability of 3D-printed dentures.
Methods: The PUF microcapsules containing TEGDMA as core material were synthesized in oil-in-water emulsion and characterized for size, surface morphology and thermal stability. 3D-printed denture base resin with 0, 5, 15, and 25 wt% content of the synthesized PUF were printed and evaluated by degree of conversion, surface morphology, topography, surface hardness, flexural strength, fracture toughness, self-healing efficiency, and fluorescent microscopic visualization of the microcracks' self-healing event through the in-situ release of rhodamine B labelled healing agent from ruptured PUF microcapsules inside the resin matrices.
Results: As compared to the control, a slight decrease was observed in the degree of conversion, surface hardness and flexural strength of the 3D-printed denture base composite modified with the PUF microcapsules. Results demonstrated that an increase in the microcapsule content significantly ($p \leq 0.05$) enhances the fracture toughness and self-healing efficiency. The HPLC results analysis of the experimental groups demonstrated a controlled release profile of healing agent over time with the maximum release on day 7. The microscopic visualization findings demonstrated the successful encapsulation and intentional triggered release of the rhodamine B. labelled healing agent in the crack plane.
Significance: The 3D-printed denture base resin composites modified with the PUF microcapsules showed a significant potential for microcrack self-healing and enhanced fracture toughness based on the content (wt%) of microcapsules.

1. Introduction

Additive manufacturing, also known as 3D printing or rapid prototyping (RP), has revolutionized the field of modern dentistry by producing highly accurate 3D-printed restorations and prostheses [1–5]. 3D-printed dentures offer significant advantages over traditional dentures due to the faster process with fewer fabrication stages and steps, digitized workflow, reduced number of appointments, improved tissue adaptation, and straightforward duplication of existing dentures [6]. However, among the main reasons for the clinical failure of resin-based prosthetic restorations, including the dentures, is the formation and accumulation of micro-cracks due to the harsh oral environment including masticatory forces and thermal stresses [7]. Therefore, arresting cracks at micro level is of utmost importance to enhance the mechanical longevity of resin-based prostheses.

Attempts have been made to develop dental resin composites with improved resistance to mechanical failures and fracture through imparting self-healing capabilities. A self-healing system is based on the incorporation of a microencapsulated healing agent with the potential to repair generated cracks and recover the mechanical performance to a

* Correspondence to: Dental School, The University of Western Australia, 17 Monash Avenue, Nedlands, WA 6009, Australia.
E-mail address: amr.fawzy@uwa.edu.au (A. Fawzy).

https://doi.org/10.1016/j.dental.2025.02.003
Received 11 September 2024; Received in revised form 16 January 2025; Accepted 11 February 2025
Available online 14 February 2025

certain extent [8]. The process of encapsulating solids, liquids, or gaseous molecules in tiny, sealed capsules that may release their contents at a precise and controlled rate under triggered circumstances is known as microencapsulation [9,10]. In dentistry, self-healing microcapsules were mainly investigated for *in-situ* repair of bonding resins, coatings, and direct restorative resin-based composites [11–13]. Researchers have used either polyurea formaldehyde or silica-based microcapsules with the main healing agents being dimethacrylate based monomers [11,14–19]. Other studies have used polyacids or water, loaded to the core of the microcapsules, as healing agents [20]. While self-healing strategies have been extensively explored for direct resin-based dental restorative composites, their application in 3D printed dental prostheses has remained underexplored. Self-healing strategies could enhance the mechanical durability and consequently the clinical lifespan of 3D-printed dental resin-based composites restorations and/or prothesis, such as dentures, through imparting an *in-situ* auto repairing mechanism for minor cracks during clinical service.

The aim of this laboratory study was to develop and characterize 3D-printed resin composites containing self-healing polyurea formaldehyde (PUF) microcapsules for arresting microcracks formation and enhancing the mechanical durability of 3D-printed dentures through imparting an *in-situ* self-healing mechanism. The first objective was to synthesize and characterize polyurea formaldehyde (PUF) microcapsules filled with a triethylene glycol dimethacrylate (TEGDMA) base resin and 1 % N,N-*bis* (2-hydroxyethyl)-p-toluidine (DHEPT) through *in-situ* polymerization technology. The second objective was to formulate and characterize dimethacrylate-based 3D-printed resin composites modified with varying weight contents of the self-healing PUF microcapsules. The modified experimental 3D-printed composites were characterized for their surface morphology, topography, hardness, flexural strength, fracture toughness, and self-healing efficiency. The third objective was to study the self-healing process by characterizing the healing agent release from the 3D-printed composites. In addition, to microscopically visualizing the microcracks' self-healing event through the *in-situ* release of the rhodamine B labelled healing agent from the ruptured PUF microcapsules inside the resin matrices. The null hypotheses were 3D-printed denture base composites modified with the self-healing PUF microcapsules exhibit no significant improvement in mechanical properties and self-healing potential compared to the unmodified conventional 3D-printed denture base resin alternative.

2. Materials and methods

All chemicals and precursors used in this study were of analytical grade and used as such without further purification: ethylene maleic anhydride, urea, ammonium chloride, resorcinol, sodium hydroxide, triethylene glycol dimethacrylate, benzoyl peroxide, N,N-diethyl-p-toluidine (DHEPT) and formaldehyde solution were purchased from Sigma Aldrich. The used 3D-printed denture base resin material (Next-Dent, NDD3LP01000_1, Netherlands) is formed of ethoxylated bisphenol A dimethacrylate (≥ 75), 7,7,9-trimethyl-4,13-dioxo-3,14-dioxa-5,12-diazahexadecane-1,16-diyl bismethacrylate (or 7,9,9-trimethyl-4,13-dioxo-3,14-dioxa-5,12-diazahexadecane-1,16-diyl bismethacrylate (10–20), 2-hydroxyethyl methacrylate (5–10), silicon dioxide (5–10), diphenyl(2,4,6-trimethylbenzoyl) phosphine oxide (1–5), and titanium dioxide (< 0.1) (Material's Safety Data Sheet).

2.1. Synthesis and characterizations of the polyurea formaldehyde (PUF) microcapsules

The self-healing microcapsules were formulated by *in-situ* polymerization of formaldehyde and urea following a previous protocol with modification [21]. Briefly, 2.5 g urea, 0.25 g ammonium chloride and 0.25 g resorcinol were mixed in 100 mL of deionized water containing 25 mL of 2.5 % aqueous solution of ethylene maleic anhydride (surfactant) in a 500 mL round bottom glass flask placed in a water bath at room temperature under continuous magnetic stirring. The pH was monitored by a pH meter (Eutech™ pH 700 Meter, ThermoFisher Scientific, Australia) and maintained from 2.4 to 3.5 by drop-wise addition of 2 M sodium hydroxide solution. The 60 mL of core solution (1 wt% DHEPT and 99 wt% TEGDMA) was added dropwise in the shell solution and the stirring speed was raised to 400RPM to make a stable emulsion of DHEPT-TEGDMA droplets. After 15 min, 6.33 g of formaldehyde solution was added dropwise, and the temperature was raised to 55 °C at the rate of 10 °C/min. The flask was covered with aluminum foil to prevent evaporation and the reaction was left and monitored in hourly-bases for the formation of microcapsules using a light microscope and Fourier-Transform Infrared Spectroscopy (IR-Spirit®, Shimadzu, Japan). The obtained microcapsules were rinsed with distilled water and then iso-propanol repeatedly, vacuum filtered and left in a closed fume hood for 24 h for air drying.

The obtained free-flowing microcapsules fine powder was characterized for size, structure, and morphology. Particle size was determined by using Mastersizer 2000. Ver. 5.60 laser diffraction particle size analyzer (Malvern Instruments, Malvern, UK). For scanning electron microscope (SEM) imaging, the synthesized microcapsules were platinum sputtered and observed under 1555 VP-FESEM (Zeiss, Baden-Württemberg, Germany). The yield of the microcapsules was measured by dividing the total weight of the obtained microcapsules (W_{total}) by the initial weight of shell and core components (W_{shell}+ W_{core}). The fill content was recorded by following an extraction method [19,22]. Briefly, 500 mg of microcapsules were weighed and crushed in the pestle and mortar, rinsed with acetone and ethanol several times, vacuum filtered and dried at room temperature for 24 h. The resultant powder was weighed, and the encapsulated content was measured according to the following formula:

$$[(W_1\text{-}W_2)/W_1) \times 100] \quad (1)$$

where W_1 is the initial weight of the microcapsules taken and W_2 is the weight of the shell material after rinsing and drying.

Thermogravimetric (TGA) analysis was performed using STA 6000 Simultaneous Thermal Analyzer (Perkin-Elmer, Norwalk, CT, USA). The analysis was carried out at 40–800 °C at the heating rate of 10 °C.min^{-1} under an inert nitrogen environment at a flow rate of 100 mL min^{-1}.

2.2. Formulation and 3D printing of the denture base composites

The 3D printed denture base resin material was incorporated with 1 wt%. BPO as a self-healing initiator and stirred via magnetic stirring until completely homogenized. The resultant resin was loaded with varying mass fractions of dry microcapsules to form four experimental groups as shown in Table 1. The varying mass concentrations of microcapsules added in the 3D-printed resin to form self-healing experimental groups (Table 1) were selected based on the previous preliminary trials conducted to strike a balance between 3D printing parameters and effective self-healing performance without compromising key properties. The unmodified denture base resin was used as a negative control.

The modified resin mixture (from each group) was gently transferred into the digital light processing printer tray (Kulzer 3D Printer System, Australia) (Fig. 1). The light source of the 3D-printer was industrial LED with a peak wavelength of 385 nm. The STL format files of the ISO-

Table 1
Groups and composition (in wt%) of the control and modified resin composites.

Groups	3D-printed resin (wt%)	Initiator (Benzoyl peroxide) (wt%)	Self-healing Microcapsules (wt%)
Control	100	0	0
Exp−0MC	99	1	0
Exp−5MC	94	1	5
Exp−15MC	84	1	15
Exp−25MC	74	1	25

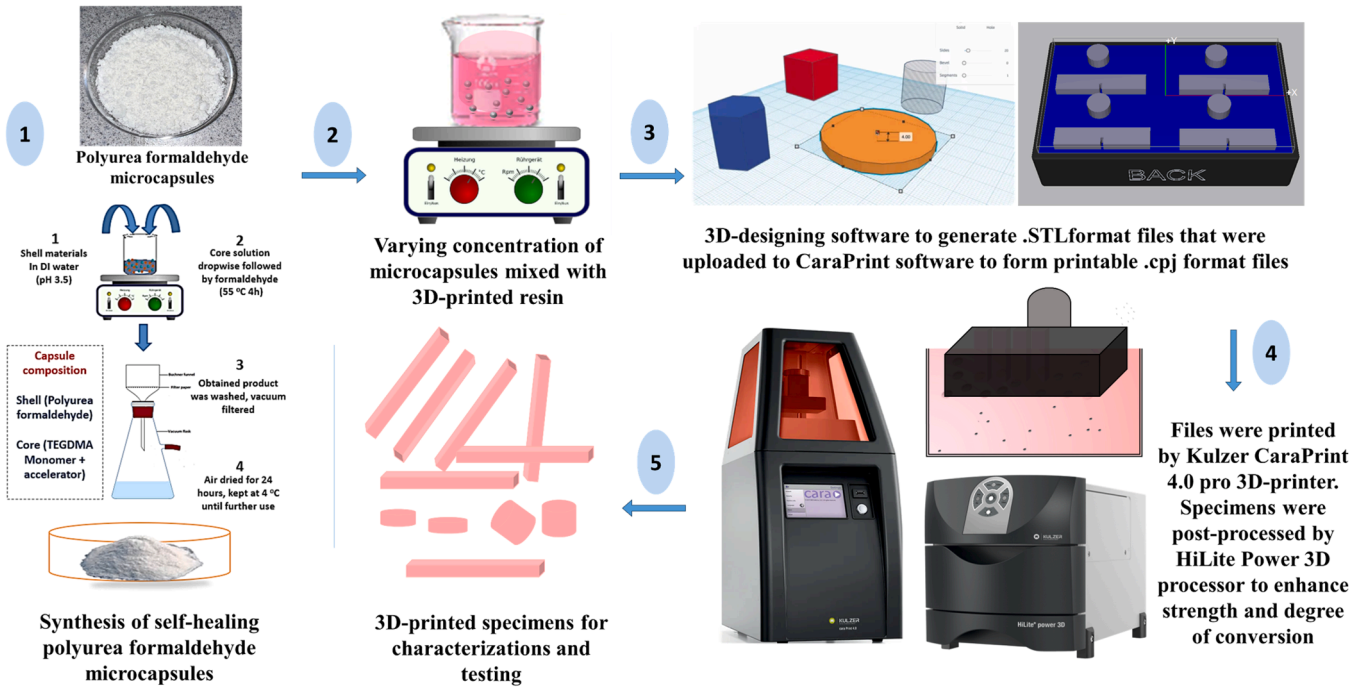

Fig. 1. Schematic diagram of the formulation and 3D printing of the self-healing experimental 3D-printed denture base composites specimens.

guided 3D-designed specimens were uploaded to the Computer Aided Design and Cara Print 4.0 software and converted to printable. cpj format files. The resolution was set at a 100 μm thickness for each layer. The polymerization time for each layer was 2 minutes approximately. Later, the printed specimens were cleaned with isopropanol for 3 min and rewashed for 2 min in ultrasonic bath. The cleaned specimens were subjected to a post-curing step to enhance the resin conversion using a high-performance light curing unit for 20 min (HiLite Power 3D; Kulzer). HiLite power 3D has a high-power flash bulb (200 W) with a wide range of light from 390 – 540 nm and rated frequency of 50–60 Hz. Finally, all the specimens were finished using ascending grit (1500–4000) silicon carbide papers followed by 1 μm diamond suspension for polishing using micro-polisher (Buehler-MetaDi, Buehler, Lake Bluff, IL, USA) under water coolant, then thoroughly rinsed with deionized water.

2.3. Characterization of the 3D printed denture base composites

2.3.1. Fourier-transformed infrared spectroscopy (FTIR) analysis

FTIR (Shimadzu Corporation, Kyoto, Japan) coupled with attenuated total reflectance (ATR-IR-Spirit®, Shimadzu, Japan) was used to determine the degree of conversion (DC) of the 3D printed composites. Spectra were collected in the mid-infrared region ranging from 4000 to 400 cm^{-1}, at a resolution of 4 cm^{-1} with an average of 32 scans at room temperature. 3D printed disc-shaped specimens (5 mm diameter and 2 mm thickness) of the control and experimental groups (n = 7) were scanned in its uncured state, and then scanned again after the final polymerisation (post-curing). The degree of conversion was measured by plotting the area of aliphatic peak (C═C) at 1638 cm^{-1}, and aromatic peak (C═C) at 1608 cm^{-1} [23]. Following formula was used:

$$DC(\%) = 100 \times (1 - R_{cured}/R_{uncured}) \quad (2)$$

R_{cured} is the ratio of polymerized aliphatic and aromatic carbon bonds, where $R_{uncured}$ is the ratio of unpolymerized aliphatic and aromatic carbon bonds.

2.3.2. Scanning electron microscopy (SEM)

3D printed disc-shaped specimens (5 mm×2 mm) (n = 5) finished and polished as previously described were used for surface morphological investigation. For analysing the fracture pattern, specimens used for fracture toughness testing were used (n = 7). Specimens were fixed on SEM stubs using copper tape and coated with a ~3 nm film of platinum using a sputter coater (Polaron SC7640, Quorum Technologies Ltd, UK). SEM (1555/VP-FESEM, Zeiss, Baden-Württemberg, Germany) was used at 5 kV accelerating voltage for imaging.

2.3.3. Atomic force microscope (AFM)

The surface microtopography and roughness of the polished disc-shaped (5 mm×2 mm) specimens (n = 5) were characterized using an atomic force microscope (Cypher S Asylum SPM, Oxford Instruments, USA). AFM investigation was performed at high resolution in the air tapping-mode using a rectangular probe (MikroMasch XSC11 Series, Innovative Solutions, Bulgaria) at an estimated frequency of 350 kHz and the nominal spring constant of 44.50. All measurements were taken with resolution of 256 line and scan speed of 2.44 Hz at room temperature. To observe the topographical changes, 3D images of composite specimens' surfaces were acquired at 20 μm^2 scan area. The average surface roughness parameter (Sa) was calculated using a specialized software (Gwyddion software 2.55).

2.3.4. Surface hardness

3D-printed disc-shaped (5 mm×2 mm) specimens (n = 9) were used for the measuring Vickers hardness number (VH) using a microhardness tester (Duramin-40; Struers, Australia). A load force of 100 g with a dwell period of 15 s was used to indent the specimen. The average of the three randomly chosen indented spots for each specimen was used to report the results.

2.3.5. Flexural strength

The flexural strength test was performed using the Instron Universal Testing Machine (ElectroPuls™ E3000; Instron USA) operated by the Bluehill 3 software. Rectangular shaped specimens (n = 13) having the dimensions of 65 mm × 10 mm× 3.3 mm were printed following the International Standards Organization (ISO; 20795–1) guidelines for denture base polymers. A flexural load was applied at the crosshead speed of 0.5 mm/min and a span width fixed at 40 mm. The ultimate

flexural strength (σ) was measured in MPa using the following formula:

$$\sigma = 3FL/2bt^2 \quad (3)$$

where F = the maximum load in Newtons (N), L = the distance between the supports (mm), b = the width of the specimen (mm), and t = the thickness of the specimen (mm).

2.3.6. Fracture toughness and Self-healing efficiency

The fracture toughness test was conducted using a single edge V-notched beam (SEVNB) method based on the peak load to fracture the specimens. According to the ISO 20795 standard, composites specimens (39 mm × 8 mm × 4 mm) having a predefined notch depth of 2 mm were designed and printed (n = 13) [24]. The notch was sharpened with the help of a razor blade using 1 μm diamond suspension prior to loading. Fracture toughness was assessed using an Instron Universal Testing Machine (ElectroPuls™ E3000, Instron USA) set at a loading speed of 0.3 mm/min. The initial fracture toughness ($K_{IC\text{-}ini}$) was calculated by using Eqs. (4) and (5). The fractured specimens were reassembled such that an intimate contact between the two fractured parts was achieved and allowed to heal at 37 °C for 48 h. The healed specimens were re-tested again using the same method, and the "heal" fracture toughness ($K_{IC\text{-}heal}$) was re-calculated using the same equations:

$$K_{IC} = f(x).F_{\max}.l_t \Big/ b_t.h_t^{\frac{3}{2}}.\sqrt{10^{-3}} \quad (4)$$

$$f(x) = 3x\frac{1}{2}[1.99 - x(1-x)(2.15 - 3.93x + 2.7x^2)] \Big/ [2(1+2x)(1-x)^{3/2}] where\ x = \frac{a}{h_t} \quad (5)$$

where F_{max} is the maximum load exerted on the specimen in newtons, "a" is the length of pre-crack in mm, "$h_t^{"}$ is the height of the specimen in mm, "$b_t^{"}$ is the width of the specimen in mm, and "$l_t^{"}$ is the span width in mm.

The healing efficiency (η) is the percentage of the healed/recovered fracture toughness ($K_{IC\text{-}heal}$) in comparison with the initial fracture toughness ($K_{IC\text{-}ini}$) and calculated using the following equation:

$$\eta = (K_{IC-heal}/K_{IC-ini} \times 100\%) \quad (6)$$

2.4. Healing agent release

A precise HPLC method was optimized and validated for the release study of the healing agent from the formulated self-healing 3D-printed denture base composites. The standard solution and specimens were assessed by Agilent 1260 HPLC system with an Altima C_{18} phase column serial no. 21602052 (5 μm) having an internal dimeter of 2.1 mm and length of 150 mm. The mobile phase was water and acetonitrile (60:40 vol./vol.). The flow rate of 10 μL injection was adjusted at 0.4 at mL/min, and the eluents were monitored at λ_{max} of 230 nm. Reference standard of the healing agent monomer, i.e., TEGDMA was prepared in methanol (1 mg/ mL) from the stock solution of the original monomer. The solution was then serially diluted to final calibrations of 1–1000 μg/mL (1–0.001 mg/mL). The calibration curve of reference standard was plotted relying on the known concentration (μg/mL) of healing agent monomer. The retention time (RT) of healing agent (TEGDMA resin monomer) was determined to be 7.9 min. The correlation coefficient R^2 value was found to be 0.998 suggesting a strong and reliable linear relationship between the concentrations of the standards and their response values. Disc-shaped (5 mm × 2 mm) specimens (n = 7) were prepared and stored in 5 mL deionized water at 37 °C. The solution for HPLC testing was collected periodically on day 1, 7, and 28 without any change in storage solution. The analysis was carried out by comparing the peak area of respective specimens.

2.5. Microscopic visualization of the self-healing process

To confirm the core solution was successfully encapsulated, Nikon A1RMP multiphoton microscopic investigation was conducted. To fluorescent label the core material, 15 mg of rhodamine B was added to the 60 mL of core solution (healing agent). The resulting concentration of rhodamine B in the core solution was optimized to be 0.025 %. A laser with an excitation wavelength of 631 nm was used to excite the fluorescent rhodamine B compound labelled to the healing agent and observed under the Nikon PlanApo objective of 10 × in air-mode. To further visualize the microcapsules rupture and healing agent release with crack propagation, a thin film of light-cured unfilled dimethacrylate based resin monomer (Sigma Aldrich, St. Louis, MO, USA) was applied on the glass slide and a small number of fluorescent-labelled microcapsules were sprinkled on and embedded in the resin thin film. After light curing with visible light curing device (Ivoclar Vivadent, Bluephase style, Liechtenstein) for 20 s, the cured resin film was cut in a crisscross manner with the help of a surgical blade #23 (Kai Japan, Stainless) and kept at 37 °C in incubator for 24 h. After that, the resin film was examined under the fluorescent microscope to observe the release of the labelled healing agent across the fracture line. After observing the release of the labelled healing agent from the PUF microcapsules loaded to the light-cured dimethacrylate resin matrix, fluorescent-labelled microcapsules were added to the 3D-printing denture base resin to print specimens similar to the ones used for fracture toughness testing to visualize the release of the healing agent on surfaces of the fractured parts of the healed specimens. The 3D-printed specimens were subjected to load until fracture as mentioned in section 2.2.6 and kept at 37 °C for 48 h for self-healing. Then, the healed specimens were examined under SEM and multiphoton Nikon A1RMP fluorescent microscope.

2.6. Statistical analysis

One-way ANOVA followed by the Turkey's *post hoc* test for pair-wise comparison was performed to analyze results for degree of conversion, surface roughness, microhardness, flexural strength, fracture toughness, healing efficiency, and healing agent release at a significant value preset at $p \leq 0.05$. The sample size was established by the G*Power 3.1.9.7 (HHU, Düsseldorf, Germany) calculation using the effect size of f = 0.4, α (err problem) = 0.05, power = 0.95. The results indicated that the minimum sample size for the study was 125 samples for 5 groups. Results were presented as mean ± standard deviation values and analysed by SPSS Statistics version 20.0.

3. Results

3.1. Characterizations of self-healing polyurea formaldehyde (PUF) microcapsules

Light microscopic images (Fig. 2A) of the initiation and completion of the four-hours synthesis reaction of PUF microcapsules. It can be observed that the outer black ring that indicates the shell wall became

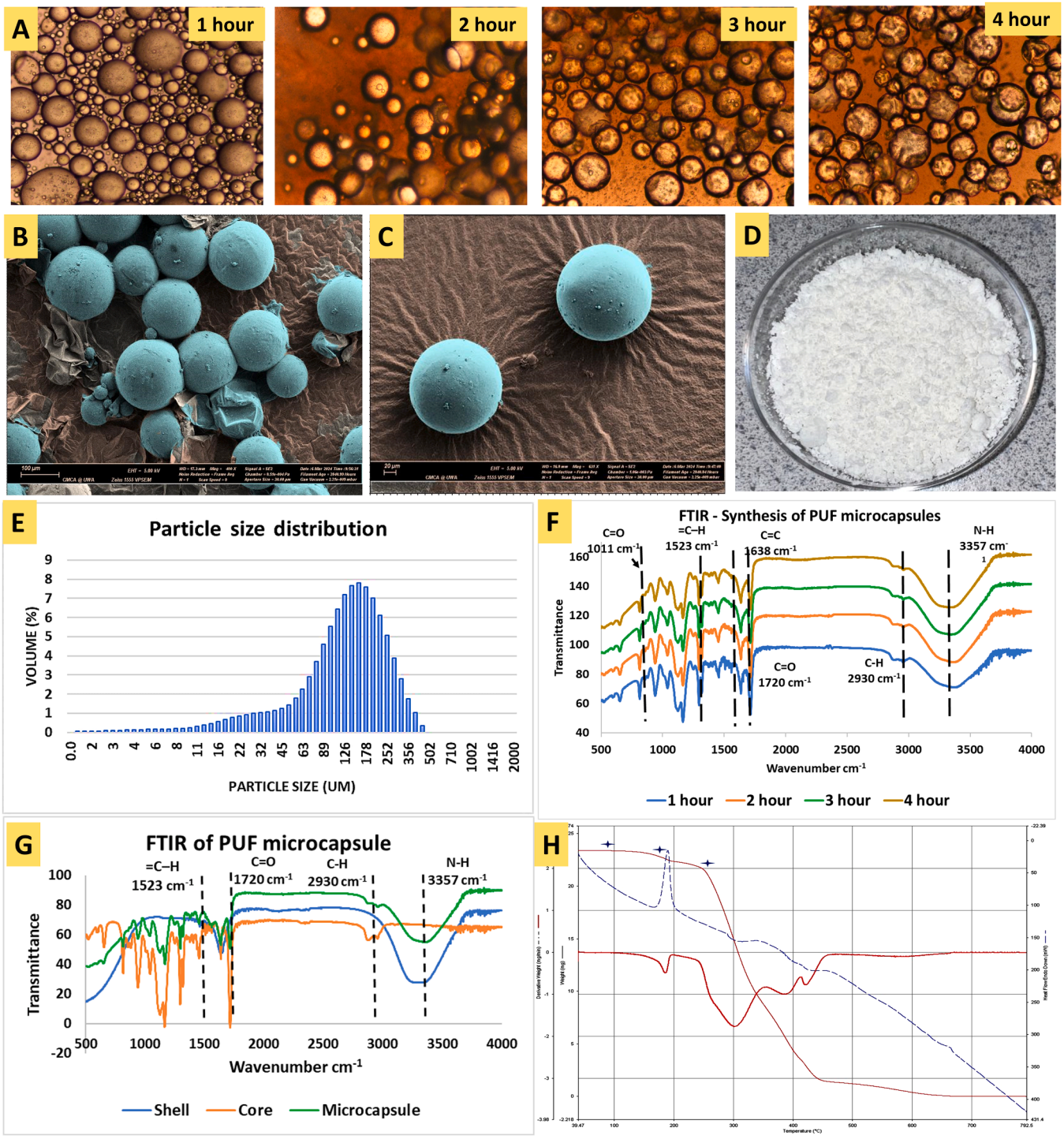

Fig. 2. (A) Light microscopic photographs representing the 4-hour reaction of PUF microcapsules synthesis where a dark outer ring indicates the end of *in situ* polymerization and encapsulation of the healing agent. (B,C) FESEM photomicrographs of PUF microcapsules showing an intact spherical shape with a smooth surface (Images have been artificially coloured for illustration using Blue Mountain software). (D) Dried PUF microcapsules. (E) Laser particle diffraction distribution curve showing the size range of the PUF microcapsules. (F, G) FTIR spectra of the PUF microcapsules' 4-hour synthesis reaction. (G) FTIR spectra of the synthesized microcapsule showing distinctive peaks of shell and core components (H) Thermogravimetric (TGA) graph of PUF microcapsules showing the thermal transitions.

denser with each hour, while the moderately brighter area interiorly indicates the healing agent became brighter. The characteristic irregular brain-skin like collapse surface feature (Fig. 2A, at 4h) is representing the slow evaporation of the solvent and complete encapsulation of TEGDMA droplets. The FESEM images of the synthesized microcapsule (Fig. 2B) shows an intact spherical shape and an apparent smooth surface with some debris associated with polyurea formaldehyde. At a higher magnification (Fig. 2C) the microcapsules appeared to be dense and having uniform size and morphology with undetectable defects or porosities. When completely dried, the polyurea formaldehyde microcapsules encapsulating TEGDMA-DHEPT had an appearance of a free-flowing white powder with little agglomeration (Fig. 2D). The size of the microcapsules was analyzed by laser particle diffraction method (Fig. 2E) revealing that the most common particle size range being

150–200 μm and having polydispersity index of 1.3. The variation in chemical composition of the microcapsules with the synthesis process was analyzed by FTIR (Fig. 2F) revealing the characteristic spectral peaks corresponding to specific functional groups present in the PUF microcapsules. The stretching vibration peak at 1720 cm^{-1} (C═O), 1638 cm^{-1} (C═C), and the peak for methylene group -CH_2 at 2800–3000 cm^{-1} (Fig. 2F) are following an hourly linear decreasing trend indicating the encapsulation of TEGDMA monomer by urea and formaldehyde. However, the peaks at 3357 cm^{-1} (-NH) and 1559 cm^{-1} (-CN) are the characteristic absorption peaks indicating the formation of PUF shell wall surrounding the healing agent, respectively [25]. (Fig. 2G) is displaying FTIR spectra of the distinctive peaks of shell and core component present in the synthetized PUF microcapsule (MC) confirming a successful encapsulation of the healing agent inside the microcapsules [26]. Moreover, the TGA curve (Fig. 2H) is illustrating the thermal transitions revealing the decomposition behaviour of the microcapsules. It is noteworthy that microcapsules remained stable until approximately 120°C, after which a slight weight loss was observed, mainly due to the evaporation of unreacted formaldehyde and residual water and [27]. A significant thermal reduction occurred at 248 °C that corresponds with the boiling temperature of the TEGDMA (core) as the main component of the microcapsules. Another significant weight loss appeared around 320 °C due to the degradation of highly cross-linked PUF (shell) of microcapsules [26,28,29]. The yield and fill content of the microcapsules were estimated to be 71.2 % and fill content was 56.2 %, respectively.

3.2. Characterization of the 3D-printed denture base composites

3.2.1. FTIR and the degree of conversion

Fig. 3(A) shows typical FTIR spectral lines of the 3D printed control and experimental specimens where the peak heights at the wave numbers of 1637 cm^{-1} and 1608 cm^{-1} were used to calculate the degree of conversion (DC; Fig. 3B). There was no significant difference between the control and Exp-0MC, Exp-5MC and Exp-15MC, and Exp-15MC groups. However, a significant decrease was found between the control and Exp-25MC group.

3.2.2. Morphology and surface topography

Three-dimensional reconstructed AFM images of the surface microtopography of the unmodified (control) along with the PUF-modified experimental 3D-printed composites are shown in (Fig. 4A). From the AFM images, an increase in surface texture/roughness can be observed with increasing the content of microcapsules. This is confirmed with the Sa roughness parameter results (Fig. 4B) showing a gradual increase in the Sa roughness parameter value. A significant difference was observed among all groups ($p \leq 0.05$), where the lowest Sa value was observed for the control, whereas Exp-25MC group showed the highest value. Both AFM and surface roughness results were in accordance with SEM findings, where the control, Exp-0MC and Exp-5MC showed the smooth surface texture without any observable surface defects (Fig. 4C-E). However, the increase in microcapsules content in the resin matrices (Exp-15MC and Exp-25MC) led to randomly located round defects of approximately 100–150 μm in diameter on the surface indicating the locations of fractured/ruptured microcapsules (Fig. 4F, G).

3.2.3. Mechanical properties and self-healing efficiency

Surface microhardness results are presented as means ± SD VHN values for all groups (Fig. 5A). A significant increase in VHN was only found with the Exp-0MC and Exp-5MC groups compared to the control. With the increase in the microcapsule content, as shown in the Exp-15MC and Exp-25MC experimental groups, no difference in VHN compared to the control group was found. The means ± SD of flexural strength of the 3D printed composites are presented in Fig. 5B. A significant difference ($p \leq 0.05$) was observed among all groups except between control and Exp-0MC. In addition, the increase in microcapsules content led to a significant decrease in the flexural strength.

The means ± SD of the initial and healed fracture toughness are presented in (Fig. 5C). It was found that only composite specimens having a microcapsule content of 15 wt% (Exp-15MC) led to a significant increase in the initial fracture toughness ($K_{IC\text{-}ini}$) compared to the control specimens ($p \leq 0.05$). However, there is no statistically significant difference between Exp-0MC, Exp-5MC and EXP-25MC with the control group. Regarding the healed fracture toughness ($K_{IC\text{-}heal}$), only the experimental groups with 5 wt%, 15 wt% and 25 wt% microcapsules contents showed healing capabilities while no values were recorded for the control and Exp-0MC groups. A significant increase was observed in the healed fracture toughness ($K_{IC\text{-}heal}$) with the increase in microcapsules contents ($p \leq 0.05$). In addition, the healing efficiency and success rate cannot be calculated for the control and Exp-0MC groups. A statistically significant difference ($p \leq 0.05$) was observed between the Exp-5MC, Exp-15MC and Exp-25MC groups (Fig. 5D). The maximum healing efficiency (39.6 %) was found with the Exp-25MC group which was decreased to (14.7 %) for the Exp-15MC group and further reduced to the minimum value (8.6 %) for the Exp-5MC group. In contrary, Exp-15MC group showed significantly higher success rate compared to the Exp-5MC and Exp-25MC groups ($p \leq 0.05$).

SEM images of the fractured, non-healed surfaces of the control and the experimental groups following fracture toughness testing are shown in Fig. 6. The SEM images of the control and Exp-0MC, having 0 wt% microcapsules, demonstrated fine textured fractured surfaces (Fig. 6A, B). On the other hand, with the incorporation of the self-healing microcapsules, especially with higher weight percentages (Exp-15MC and Exp-25MC) more textured fractures surfaces with residual ruptured

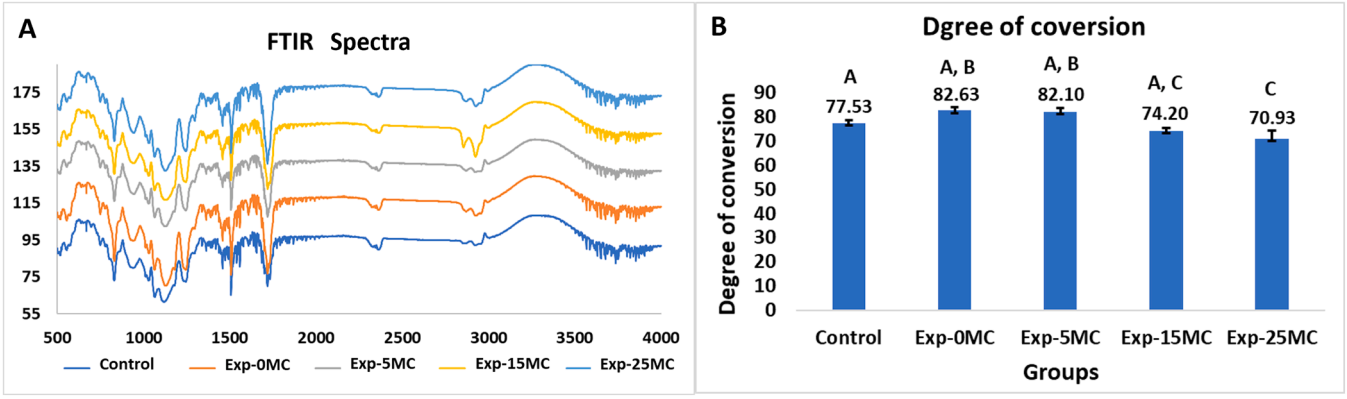

Fig. 3. (A) FTIR spectra and (B) the means ± SDs of degree of conversion (DC) of 3D-printed control and experimental composites groups (Dissimilar letters indicate statistical significance difference).

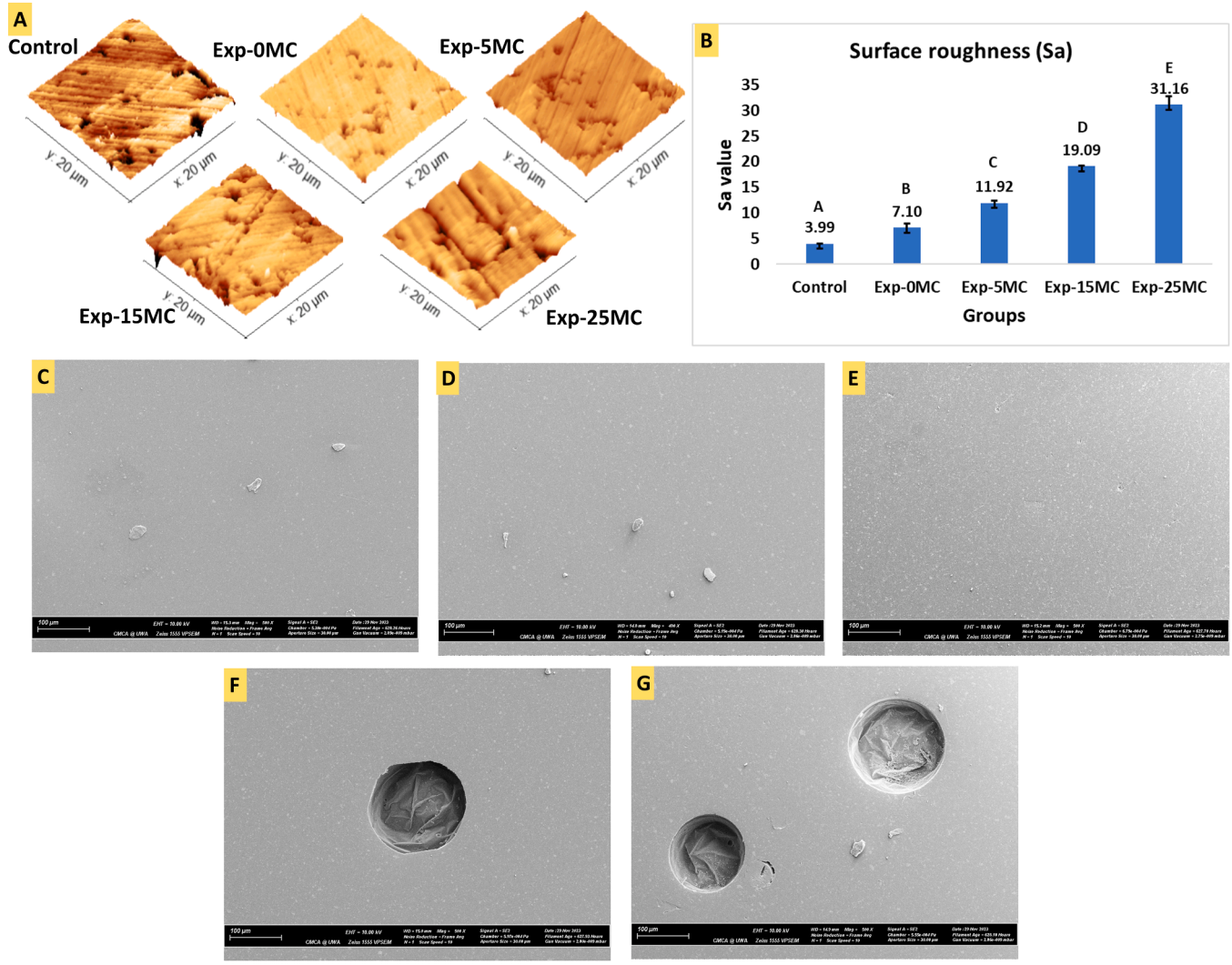

Fig. 4. (A) Representative AFM surface topographic 3D images, at the 20 µm × 20 µm scanning area obtained in tapping-mode, of the control and experimental composites groups. (B) Bar chart representing the mean ± SD of the average surface roughness (Sa) of the control and experimental groups (Dissimilar letters indicate statistical significance difference). (C-G) Representative SEM images showing the surface morphology of the control and Exp-0MC, Exp-5MC, Exp-15MC and Exp-25MC experimental groups, respectively.

microcapsules and released healing agent were observed (Fig. 6C-E).

3.3. Healing agent release profiles

The release profiles of the healing agent from the control and experimental composites groups at periodic intervals of day 1, 7, and 28 is shown in Fig. 7. No release was observed for control and Exp-0MC at any periodic interval. However, the TEGDMA characteristic peak (RT 7.9 min) was only recorded for the composites containing the self-heling microcapsules (Exp-5MC, Exp-15MC and Exp-25MC) indicating healing agent release. In addition, there was a significant increase in healing agent release with the increase in microcapsule content from 5 to 25 wt % ($p \leq 0.05$). Furthermore, no TEGDMA characteristic peak was recorded at day 1 for Exp-5MC group.

3.4. Microscopic visualization of the self-healing process

Multiphoton fluorescent microscopic images (Fig. 8A, B) showing the red fluorescence of rhodamine B. labelled TEGDMA within the microcapsules core indicating the encapsulation of the healing agent. After placing the microcapsules in the visible light cured resin and intentionally fracturing the resin film in a criss-cross manner with the blade, the rhodamine B. labelled TEGDMA can be visualized bleeding across the fracture lines (Fig. 8C) following microcapsules rupture. By loading fluorescent-labelled microcapsules in the fracture toughness specimens, a limited release of the rhodamine B. labelled TEGDMA healing agent was observed for Exp-5MC after fracturing the specimens (Fig. 8D). However, with increasing the microcapsule content up to 15 and 25 wt %, the spreading of the rhodamine B. labelled TEGDMA healing agent is clearly detected covering the entire fractured surfaces homogeneously (Fig. 8D, E). In addition, SEM images of the fractured specimens are confirming the previous finding of having a more pronounced release of the healing agent with Exp-15MC and Exp-25MC groups (Fig. 8G, H). The reaction behind the self-healing phenomenon occurred in the healed specimens is represented in Fig. 8I.

4. Discussion

This study has evaluated the effect of self-healing polyurea formaldehyde microcapsules on the 3D printed denture base resin mechanical properties and self-healing efficiency. The microcapsules were synthesized using an *in-situ* polymerization method in an oil-water emulsion. Triethylene glycol dimethacrylate monomer with 1 % N,N-*bis*(2-hydroxyethyl)-p-toluidine (TEGDMA + DHEPT) was used as the healing

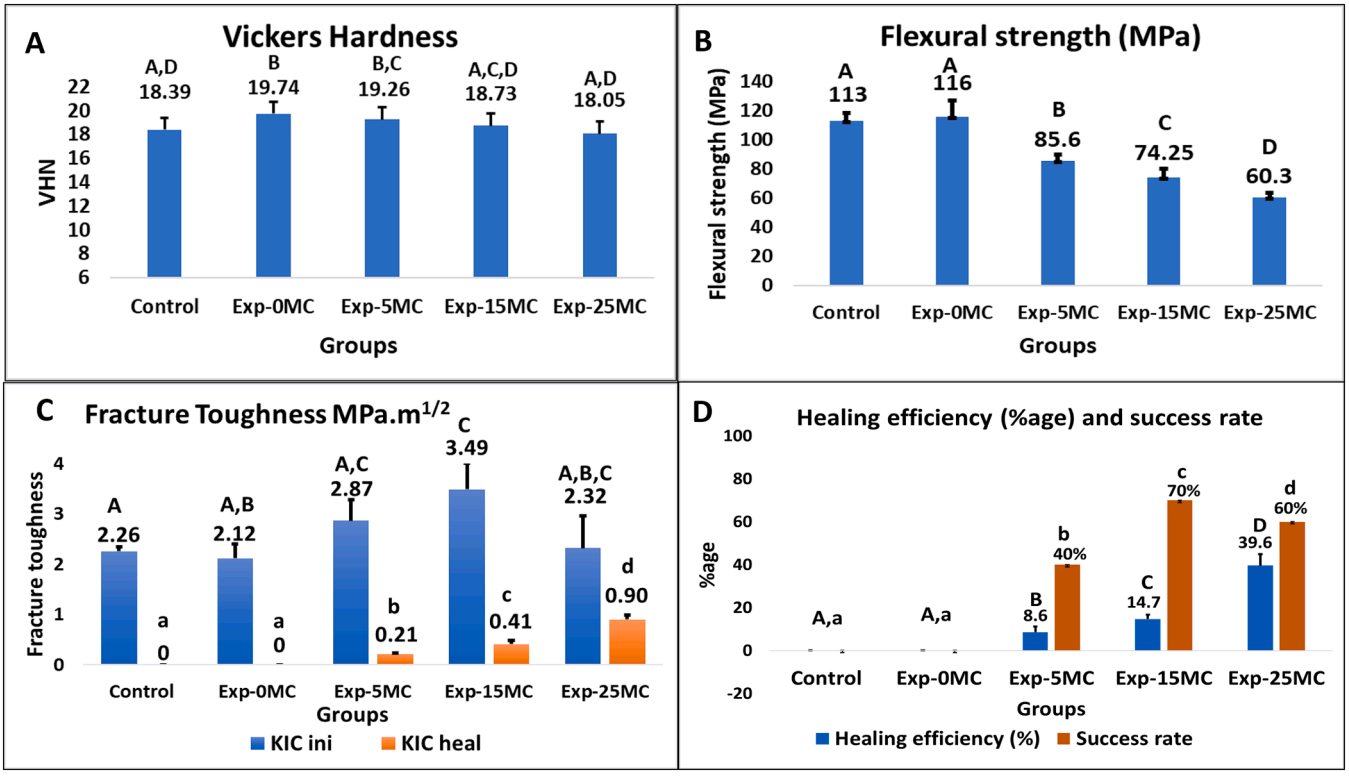

Fig. 5. Bar charts of the means ± SD values of Vickers hardness (A), flexural strength (B), and initial/ healed fracture toughness (C), and healing efficiency and success rate (D) for all 3D printed groups. Dissimilar capital or small letters indicate statistical significance difference.

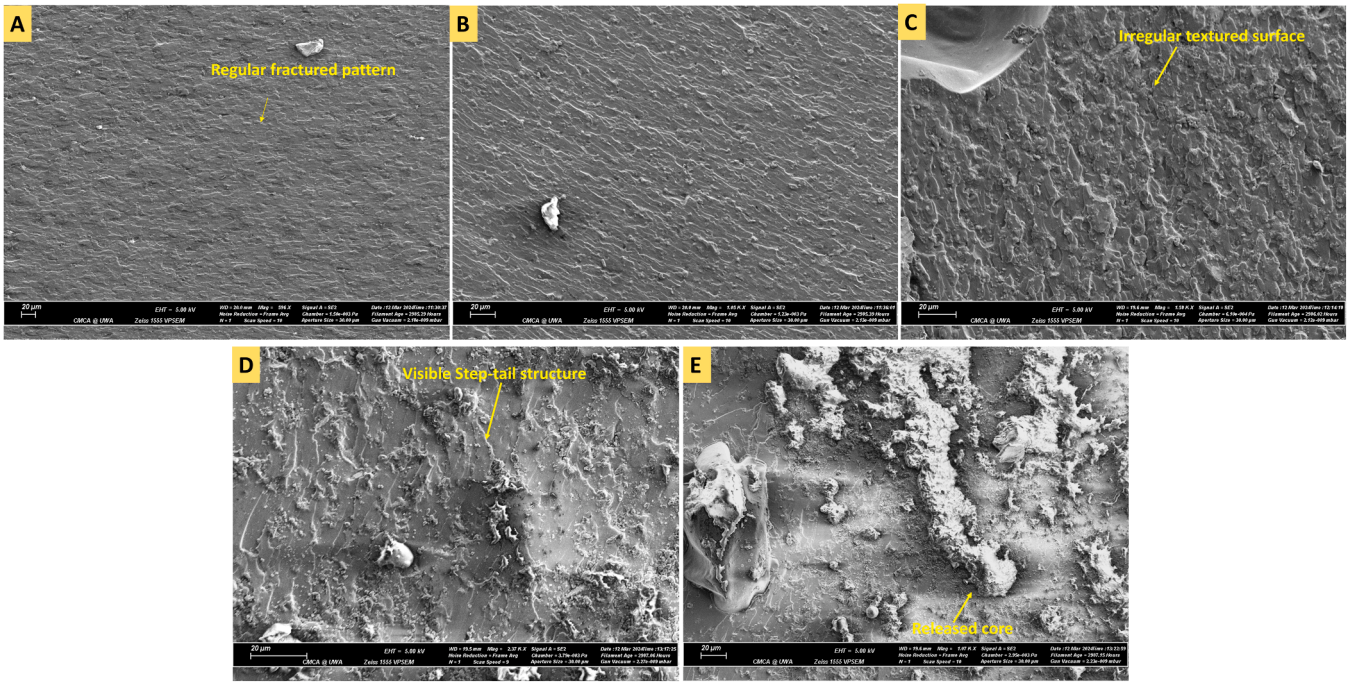

Fig. 6. (A-E) Representative SEM images of the fractured surfaces of the control (A) and the experimental 3D-printed composites specimens containing 0 % (B), 5 % (C), 15 % (D), and 25 % (E) microcapsules.

agent, while the shell was composed of polyurea formaldehyde [21,26, 30]. The primary principle involves the interfacial polycondensation of urea and formaldehyde, catalysed by ammonium chloride. This reaction forms methylolurea, which further condenses to create a three-dimensional polymeric network of polyurea formaldehyde (PUF) at the interface of the oil droplets (core solution), forming a solid shell. [31]. Light microscopic images (Fig. 2A) revealed contrast difference in the brightness of the shell and core components. This variation in the contrast can be explained by the varying refractive indices of the shell and core, where shell having high refractive index resulting in a darker

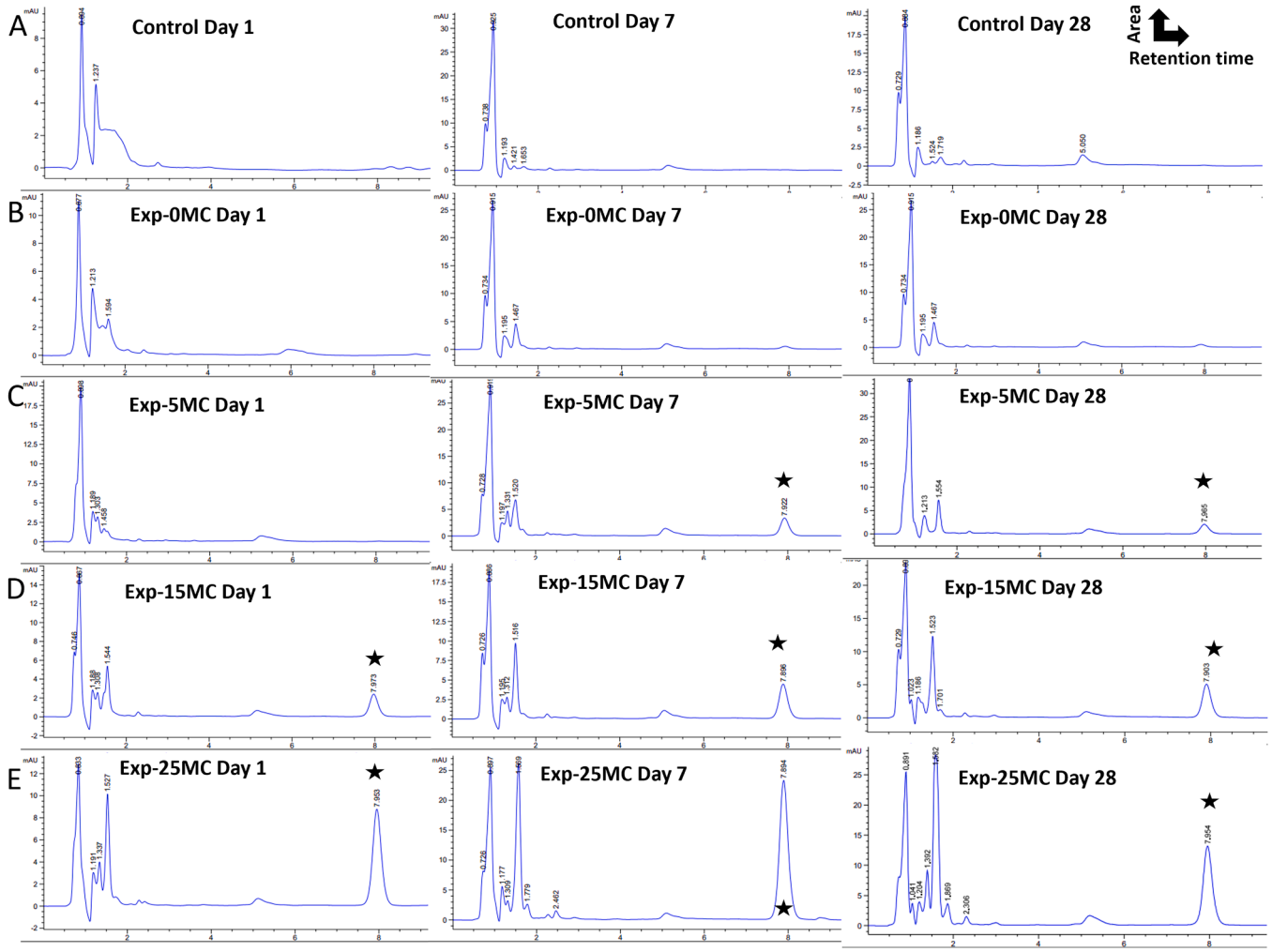

Fig. 7. HPLC results representing the healing agent release profile of unmodified 3D-printed resin (control) and 3D-printed resin with modified with 1 wt% BPO and 0, 5, 15 and 25 wt% of self-healing PUF microcapsules (Groups Exp-0MC, Exp-5MC, Exp-15MC and Exp-25MC respectively) on day 1, 7, and 28. An asterisk mark is denoting the retention time (RT) 7.9 min of TEGDMA (healing agent).

appearance and core component having low refractive index resulting in a brighter appearance [21]. This finding supports the successful synthesis of microcapsules. A key factor of a self-healing microcapsule is its rupture on crack intrusion and the subsequent release the healing agent to perform the self-healing effect. The rupturing of microcapsule is highly dependent on the morphology and size of the microcapsule. Microcapsules with the smooth surface texture (Fig. 2B, C) are less likely to agglomerate and minimize the stress concentration, leading to uniform distribution and better interfacial bonding with the matrix [32]. The size of the microcapsules can vary with changing the stirring speed; however, the size should be large enough to hold enough healing liquid and does not affect the mechanical performance. The size of the synthesized microcapsules (Fig. 2E) was around 150–200 μm at 400 rpm that is in contrast with the previous studies [19,33]. The FTIR results suggest that polyurea formaldehyde microcapsules containing TEGDMA+DHEPT (core solution) were successfully synthesized (Fig. 2F, G). The strong FTIR peak at 1711 cm^{-1} (C═O) confirms the successful encapsulation of TEGDMA monomer where the peak at the 3357 cm^{-1} (-NH) and 1559 cm^{-1} (-CN) indicates the shell formation around the core droplets [25]. Another crucial factor that affects the self-healing performance is the thermal stability of the microcapsules. It was observed that the microcapsules are stable up to 120 °C (Fig. 2H), which is lower than the temperature observed in the post processing of 3D-printed specimens. This marks an indication that the microcapsules may have survived the high processing temperatures that is in the range of 60–80 °C [34].

The synthesized polyurea formaldehyde microcapsules were added in the 3D-printed resin to formulate and characterize the 3D-printed self-healing composite. The degree of conversion (DC) of the control and experimental modified groups was measured by FTIR (3 A, B). It is noteworthy that the DC highly depends on the material composition as well as on the printing accuracy of the 3D-printer. The degree of conversion was increased upon addition of 1 wt% benzoyl peroxide and 0 wt% of microcapsules, highlighting the additional benefit of adding benzoyl peroxide on the polymerization process by offering chain-transfer reactions [35]. However, the degree of conversion decreased after increasing the amount of the microcapsules indicating the scattering of light by the microcapsules which might have adversely affected the light curing process [36].

The surface characteristics of the 3D-printed control and self-healing groups were assessed by atomic force microscopy and scanning electron microscopy (Fig. 4). Surface roughness is an integral property of denture base resin and, if not fairly smooth can lead to plaque accumulation and biofilm formation that would significantly reduce the longevity of prosthesis and also pose the patient at health risk [37]. Considering that all Sa parameter values obtained in the current study were within the ISO acceptable value of 0.2 μm for denture base prostheses (Fig. 4B), which presents no risk of plaque accumulation. However, highly polished SEM surfaces have revealed that while finishing/polishing, the microcapsules present on the surface are broken leaving behind the round defects of 100–150 μm diameter, which could lead to a fungal

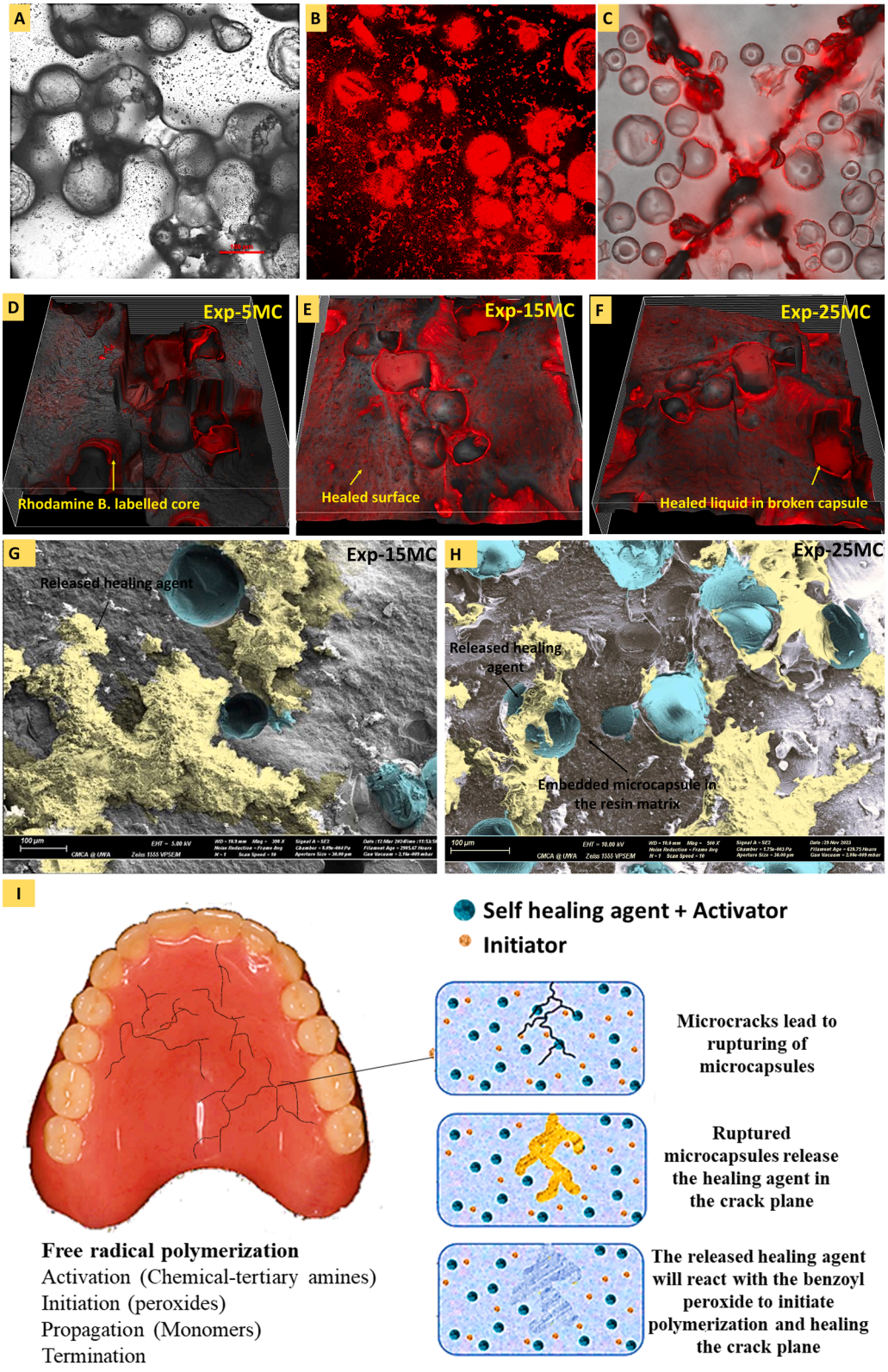

Fig. 8. Multiphoton fluorescent microscope imaging of PUF microcapsules (A,B) using two detectors: the transmittance detector (TD) showing the structure of microcapsules that is not fluorescent labelled (shell) and the RGB channel to visualize the release of the fluorescent labelled healing agent (core) from PUF microcapsules (C) The rupturing and release of the core component (healing agent) in the crack plane on a thin film of visible light cured (VLC) polymerized film. (D, E, F) Representative multiphoton fluorescent microscopic images of healed surface of 3D-printed denture resin base composite specimens containing 5 %, 15 %, and 25 % microcapsules (G, H) Representative SEM images of the healed fracture surface of Exp-15MC and Exp-25MC. Arrows indicating the released healing agent and polymerized films formed by the released healing liquid that was polymerized at the cracked plane via reaction with the initiator in the resin matrix. (I) Representation of the self-healing mechanism occurring in the microcrack planes.

attack (Fig. 4F, G). Therefore, further microbial biofilms adhesion and growth studies are recommended.

Surface hardness property of self-healing dental prostheses has not been much explored in the literature. However, the results are in consistency with the few reported studies on 3D printed denture base resin (Fig. 5A) [38,39]. According to another previous study, the addition of microcapsules up to 5 wt% has no significant effect on surface hardness as compared to the control, however, it could be decreased with increasing content of capsules more than 5 wt% [19]. The decrease in the hardness value could be related to the agglomeration of microcapsules. Increasing microcapsules content might lead to higher possibility of agglomerations to occur within the matrix, thus creating a weak region in the resin matrix leading to decreased mechanical properties. It has also been reported that surface hardness has a direct relation with the degree of conversion. The higher the degree of conversion, the better will be the polymerization and intermingling of polymer chains leading to less surface voids, increased surface homogeneity and hardness as shown by the Exp-0MC group free from microcapsules (Figs. 3B, 5A) [40]. Flexural strength is a key mechanical property that can facilitate in forecasting the performance of brittle materials. It is the ultimate stress that cause the material to fracture and is significantly dependent on the flaws and surface defects of the tested material [41]. The flexural strength results (Fig. 5B) suggested that control and experimental groups had successfully met the minimum required strength of denture base material (ISO 20795–1) ($\geq$ 60 MPa) [42]. A significant reduction in flexural strength was observed with increasing the content of microcapsules as compared to the control group (Fig. 5B). The decreased flexural strength could be due to the agglomeration of microcapsules which resulted in the unhomogenized load transfer [43]. In addition, the 3D-printing orientation and accuracy could have a potential effect on the mechanical properties, specifically flexural strength. A previous study reported that the highest flexural strength was found in specimens built with a layer orientation parallel to the axial load (90°), compared to those built at 45° or 0° [44]. It is also noteworthy to mention that the silanization of microcapsules could improve the flexural strength and interfacial bonding by facilitating the efficient stress transfer through interphases and making the composite to act as one solid unit [25,45,46].

Fracture toughness (K_{IC}) is a critical stress intensity factor that provides information on the resistance of a material to resist crack propagation [47]. In the present study, an increase in the initial fracture toughness has been observed with an increase in the microcapsule content up to 15 wt%, and then a slight decrease up to 25 wt% (Fig. 5C). These results are also consistent with the previously reported studies regarding the $K_{IC\text{-}ini}$ [21,48–51]. Increased fracture toughness could be the result of a uniform distribution and stronger bonding of the microcapsules with the resin matrix [52]. In addition, it could also be due to the "particle bridging" effect as the irregular textured fractured surface indicates more energy consumed by the specimen to fracture. The tail structure feature (Fig. 6D, E) presents on the fractured surfaces could have changed the route of crack plane when it faced the microcapsule on its way of propagation which might have increased energy consumption leading to an increase in $K_{IC\text{-}ini}$ [53]. Additionally, branched fracture line give specimen more time to fracture and delay the failure comparatively. Huyang G., et al., reported that the initial fracture toughness remained constant up to 5 wt% of microcapsule content and then decreased significantly at 15 wt% microcapsule addition in the resin matrix [20]. The possible reason behind this decreased fracture toughness could be the poor bonding of microcapsules with the resin matrix causing the capsules to act as voids instead of a filler. Nevertheless, there are several studies that have reported no significant difference in the initial fracture toughness after the incorporation of microcapsules [21,54,55]. The results of healed fracture toughness $K_{IC\text{-}heal}$ (Fig. 5C), and healing efficiency (Fig. 5D) indicate that the self-healing efficiency increased with the increase of the microcapsule content, which could be due to a higher release of the healing agent, resulting in re-bonding of the fractured/cracked planes. The maximum healing efficiency was observed to be 39.6 % for 25 wt% of microcapsule content which is a little less than observed for light-cured resin-based dental composites for the same content of microcapsules [20]. Various technical factors including the composition of 3D-printing NextDent resin, printing orientation, layer thickness, accuracy, and post curing time play a significant role in self-healing efficiency. In addition, the polyurea formaldehyde capsules were observed to settle down to the bottom part of the printing tray because of the gravity and density affecting the self-healing performance [56,57]. The increased mass concentration of microcapsules increased the viscosity of 3D-printed resin. Higher viscosity might have affected the flow and printing speed. It could also have resulted in weak interlayer adhesion and compromised mechanical properties. However, this was addressed by increasing post-processing time by 2 minutes.

The effect of possible leakage/release of the healing agent from PUF microcapsule shells needs to be analyzed. The HPLC analysis was primarily aimed to evaluate the elution of the healing agent (TEGDMA resin monomer) from 3D-printed self-healing denture base resin specimens (Fig. 7), which has not been studied previously. The results revealed that regardless of the percentage (wt%) of the self-healing microcapsules, the minimum release was observed on day 1 while maximum release was recorded on day 7, followed by a gradual decrease over time. This is suggesting a steady release profile of the healing agent, favouring the intended function of the self-healing composite. However, the gradual decrease in healing agent release after a month interval, might reflect the consumption of the healing agent released from the microcapsules into the resin matrix over time, stimulating further investigation on the sustainability of the self-healing effect. The leaching of the resin monomer also depends on the chemical structure and size of the substance, where TEGDMA being light weight (286.32), as compared to other high molecular weight monomers (bisGMA 512, UDMA 480), is more vulnerable to leach through polymeric chains, which is somehow favourable for the flow of TEGDMA monomer into the microcrack plane for healing purpose [58].

The successful encapsulation and intentional triggered release of rhodamine B. labelled core (healing agent) in the crack plane demonstrates the effectiveness of microcapsules structure and design. The microscopic visualization (Fig. 8) findings confirm that the microcapsules can release their contents in response to the physical damage, which is a crucial factor in self-healing performance. Moreover, it also indicates that the microcapsules were able to store and protect the healing agent until activation. These interesting findings support the potential effectiveness of these self-healing microcapsules when there is a damage-triggered repair. The microscopic images of the fractured, healed surfaces (Fig. 8D-H) revealed also the presence of ruptured microcapsules with numerous polymeric films suggesting that the DHEPT accelerator present in the healing agent could have reacted with BPO initiator present in the resin matrix of the 3D-printed composite successfully [21]. Fig. 8I is representing the mechanism and reaction behind the self-healing phenomenon occurred in the crack planes of the healed specimens (Fig. 8D-H).

With few limitations, the formulation of the self-healing 3D-printed denture base resin composites has been successfully achieved. Therefore, the null hypotheses were partially met. However, further research addressing the sustainability of the self-healing effect with the associated optimization of the self-healing microcapsules, closer simulation of oral conditions during the *in vitro* characterization including thermal and mechanical fatigue, and studying the biological consequences associated with self-healing modifications is required to accelerate the technology transition from lab to clinical practice.

5. Conclusion

The 3D-printed denture base resin composites modified with the PUF microcapsules showed a significant potential for microcrack self-healing

and enhanced fracture toughness. However, the self-healing efficiency is dependent on the microcapsule content. Although the flexural strength and surface hardness showed a slight decrease with adding PUF microcapsules, they remain within the ISO acceptable range of denture base resins.

Declaration of Competing Interest

The authors declare that they have no known competing financial interests or personal relationships that could have appeared to influence the work reported in this paper.

Acknowledgments

This work was supported by the Australian Dental Research Foundation (ADRF) [Grant Application No. PJ0000018]. The authors acknowledge the facilities, scientific, and technical assistance of Microscopy Australia at the Centre for Microscopy, Characterisation & Analysis, The University of Western Australia, a facility funded by the University, State, and Commonwealth Governments.

References

[1] Tunchel S, Blay A, Kolerman R, Mijiritsky E, Shibli JA. 3D printing/additive manufacturing single titanium dental implants: a prospective multicenter study with 3 years of follow-up. Int J Dent 2016;2016:8590971. https://doi.org/10.1155/2016/8590971.
[2] Javaid M, Haleem A, Kumar L. Current status and applications of 3D scanning in dentistry. Clin Epidemiol Glob Health 2019;7:228–33. https://doi.org/10.1016/j.cegh.2018.07.005.
[3] Van Assche N, Van Steenberghe D, Guerrero ME, Hirsch E, Schutyser F, Quirynen M, et al. Accuracy of implant placement based on pre-surgical planning of three-dimensional cone-beam images: a pilot study. J Clin Periodo 2007;34:816–21. https://doi.org/10.1111/j.1600-051X.2007.01110.x.
[4] Kapos T, Evans C. CAD/CAM technology for implant abutments, crowns, and superstructures. Int J Oral Maxillofac Implants 2014;29:117–36. https://doi.org/10.11607/jomi.2014suppl.g2.3.
[5] Harris BD, Nilsson S, Poole CM. A feasibility study for using ABS plastic and a low-cost 3D printer for patient-specific brachytherapy mould design. Austral Phys Eng Sci Med 2015;38:399–412. https://doi.org/10.1007/s13246-015-0356-3.
[6] Bilgin MS, Baytaroğlu EN, Erdem A, Dilber E. A review of computer-aided design/computer-aided manufacture techniques for removable denture fabrication. Eur J Dent 2016;2:286–91. https://doi.org/10.4103/1305-7456.178304.
[7] Baran G, Boberick K, McCool J. Fatigue of restorative materials. Crit Rev Oral Biol Med 2001;12:350–60. https://doi.org/10.1177/10454411010120040501.
[8] White SR, Sottos NR, Geubelle PH, Moore JS, Kessler MR, Sriram SR, et al. Autonomic healing of polymer composites. Nature 2001;409:794–7. https://doi.org/10.1038/35057232.
[9] Anal AK, Stevens WF. Chitosan-alginate multilayer beads for controlled release of ampicillin. Int J Pharm 2005;290:45–54. https://doi.org/10.1016/j.ijpharm.2004.11.015.
[10] Anal AK, Singh H. Recent advances in microencapsulation of probiotics for industrial applications and targeted delivery. Trends Food Sci Techno 2007;18:240–51. https://doi.org/10.1016/j.tifs.2007.01.004.
[11] Wertzberger BE, Steere JT, Pfeifer RM, Nensel MA, Latta MA, Gross SM. Physical characterization of a self-healing dental restorative material. J Appl Polym Sci 2010;118:428–34. https://doi.org/10.1002/app.31542.
[12] Yue S, Wu J, Zhang Q, Zhang K, Weir MD, Imazato S, et al. Novel dental adhesive resin with crack self-healing, antimicrobial and remineralization properties. J Dent 2018;75:48–57. https://doi.org/10.1016/j.jdent.2018.05.009.
[13] Ouyang X, Huang X, Pan Q, Zuo C, Huang C, Yang X, et al. Synthesis and characterization of triethylene glycol dimethacrylate nanocapsules used in a self-healing bonding resin. J Dent 2011;39:825–33. https://doi.org/10.1016/j.jdent.2011.09.001.
[14] Kafagy DH. Synthesis and Characterization of Microcapsule-Based Self-Healing Dental Composites. The University of Tulsa; 2017.
[15] Sharma A, Alam S, Sharma C, Patnaik A, Kumar SR. Static and dynamic mechanical behavior of microcapsule-reinforced dental composite. P I Mech Eng L-J Mat 2019;233:1184–90. https://doi.org/10.1177/1464420717733.
[16] Then S, Neon GS, Abu Kasim NH. Performance of melamine modified urea–formaldehyde microcapsules in a dental host material. J Appl Polym Sci 2011;122:2557–62. https://doi.org/10.1002/app.34361.
[17] Wu J, Weir MD, Melo MA, Xu HH. Development of novel self-healing and antibacterial dental composite containing calcium phosphate nanoparticles. J Dent 2015;43:317–26. https://doi.org/10.1016/j.jdent.2015.01.009.
[18] Yahyazadehfar M, Huyang G, Wang X, Fan Y, Arola D, Sun J. Durability of self-healing dental composites: a comparison of performance under monotonic and cyclic loading. Mater Sci Eng C Mater Biol Appl 2018;93:1020–6. https://doi.org/10.1016/j.msec.2018.08.057.
[19] Althaqafi KA, Satterthwaite J, Silikas N. A review and current state of autonomic self-healing microcapsules-based dental resin composites. Dent Mater 2020;36:329–42. https://doi.org/10.1016/j.dental.2019.12.005.
[20] Huyang G, Debertin AE, Sun J. Design and development of self-healing dental composites. Mater Des 2016;94:295–302. https://doi.org/10.1016/j.matdes.2016.01.046.
[21] Wu J, Weir MD, Zhang Q, Zhou C, Melo MA, Xu HH. Novel self-healing dental resin with microcapsules of polymerizable triethylene glycol dimethacrylate and N,N-dihydroxyethyl-p-toluidine. Dent Mater 2016;32:294–304. https://doi.org/10.1016/j.dental.2015.11.014.
[22] Rajasekaran SP, Huynh B, Fugolin APP. Tailoring microemulsification techniques for the encapsulation of diverse cargo: a systematic analysis of poly (Urea-Formaldehyde) microcapsules. J Funct Biomater 2024;15:117. https://doi.org/10.3390/jfb15050117.
[23] Khalid H, Syed MR, Rahbar MI, Iqbal H, Ahmad S, Kaleem M, et al. Effect of nano-bioceramics on monomer leaching and degree of conversion of resin-based composites. Dent Mater 2018;37:940–9. https://doi.org/10.4012/dmj.2017-338.
[24] Iso, I.S.O., 20795-1: 2013 Dentistry—Base Polymers—Part 1: Denture Base Polymers. ISO: Geneva, Switzerland, 2013.
[25] Li Haiyan, Wang Rongguo, Hu Honglin, Liu Wenbo. Surface modification of self-healing poly (urea-formaldehyde) microcapsules using silane-coupling agent. Appl Surf Sci 2008;255:1894–900. https://doi.org/10.1016/j.apsusc.2008.06.170.
[26] Ahangaran F, Navarchian AH. Towards the development of self-healing and antibacterial dental nanocomposites via incorporation of novel acrylic microcapsules. Dent Mater 2022;38:858–73. https://doi.org/10.1016/j.dental.2022.04.004.
[27] Yuan L, Liang G, Xie J, Li L, Guo J. Preparation and characterization of poly (urea-formaldehyde) microcapsules filled with epoxy resins. poly 2006;47:5338–49. https://doi.org/10.1016/j.polymer.2006.05.051.
[28] Katoueizadeh E, Zebarjad SM, Janghorban K. Investigating the effect of synthesis conditions on the formation of urea–formaldehyde microcapsules. J Mater Res Technol 2019;8:541–52. https://doi.org/10.1016/j.jmrt.2018.04.013.
[29] Donoso R, Reina JA, Giamberini M, De La Flor S, Ferrando F, Cerruti P. Thermal and mechanical characterization of EMA-TEGDMA mixtures for cosmetic applications. Polym 2018;10:256. https://doi.org/10.3390/polym10030256.
[30] Rozza BY, El-Refai DA, Essawy HA, Alian GA. Effect of silanization of poly (urea-formaldehyde) microcapsules on the flexural strength and self-healing efficiency of an experimental self-healing dental resin composite (An in-vitro study). J Mech Behav Biomed Mater 2024;151:106372. https://doi.org/10.1016/j.jmbbm.2024.106372.
[31] Dorieh Ali, Nosrat O, Mahmoodi Manochehr, Mamaghani Antonio, Pizzi Masoud, Mohammadi Zeydi Amin moslemi. New insight into the use of latent catalysts for the synthesis of urea formaldehyde adhesives and the mechanical properties of medium density fiberboards bonded with them. Eur Polym J 2019;112:195–205. https://doi.org/10.1016/j.eurpolymj.2019.01.002.
[32] Wu J, Weir MD, Zhang Q, Zhou C, Melo MA, Xu HH. Novel self-healing dental resin with microcapsules of polymerizable triethylene glycol dimethacrylate and N,N-dihydroxyethyl-p-toluidine. Dent Mater 2016;32:294–304. https://doi.org/10.1016/j.dental.2015.11.014.
[33] Kosarli M, Bekas DG, Tsirka K, Baltzis D, Vaimakis-Tsogkas DT, Orfanidis S, et al. Microcapsule-based self-healing materials: healing efficiency and toughness reduction vs. capsule size. Compos Part B-Eng 2019;117:78–86. https://doi.org/10.1016/j.compositesb.2019.04.030.
[34] Hiremath V, Singh M, Shukla DK. Effect of post curing temperature on viscoelastic and flexural properties of epoxy/alumina polymer nanocomposites. Procedia Eng 2014;97:479–87. https://doi.org/10.1016/j.proeng.2014.12.272.
[35] Odian G. Principles of polymerization. John Wiley & Sons; 2004.
[36] Aati S, Akram Z, Ngo H, Fawzy AS. Development of 3D printed resin reinforced with modified ZrO2 nanoparticles for long-term provisional dental restorations. Dent Mater 2021;37:360–74. https://doi.org/10.1016/j.dental.2021.02.010.
[37] Bajunaid SO, Baras BH, Balhaddad AA, Weir MD, Xu HHK. Antibiofilm and protein-repellent polymethylmethacrylate denture base acrylic resin for treatment of denture stomatitis. Mater 2021;14:1067. https://doi.org/10.3390/ma14051067.
[38] Hada T, Kanazawa M, Miyamoto N, Liu H, Iwaki M, Komagamine Y, et al. Effect of different filler contents and printing directions on the mechanical properties for photopolymer resins. Int J Mol Sci 2022;23:2296. https://doi.org/10.3390/ijms23042296.
[39] Aati S, Aneja S, Kassar M, Leung R, Nguyen A, Tran S, et al. Silver-loaded mesoporous silica nanoparticles enhanced the mechanical and antimicrobial properties of 3D printed denture base resin. J Mech Behav Biomed Mater 2022;134:105421. https://doi.org/10.1016/j.jmbbm.2022.105421.
[40] de Moraes RR, Marimon JL, Schneider LF, Sinhoreti MA, Correr-Sobrinho L, Bueno M. Effects of 6 months of aging in water on hardness and surface roughness of two microhybrid dental composites. J Prosthodont 2008;17:323–6. https://doi.org/10.1111/j.1532-849X.2007.00295.x.
[41] Yilmaz H, Aydin C, Gul BE. Flexural strength and fracture toughness of dental core ceramics. J Prosthet Dent 2007;98:120–8. https://doi.org/10.1016/S0022-3913(07)60045-6.
[42] Ulmer M. Biocompatibility and mechanical/physical properties of 3D printed, milled, and conventionally processed denture base materials. (2019) Augusta University.
[43] Bleach NC, Nazhat SN, Tanner KE, Kellomäki M, Törmälä P. Effect of filler content on mechanical and dynamic mechanical properties of particulate biphasic calcium phosphate–polylactide composites. Biomater 2002;23:1579–85. https://doi.org/10.1016/s0142-9612(01)00283-6.

[44] Unkovskiy A, Bui PH, Schille C, Geis-Gerstorfer J, Huettig F, Spintzyk S. Objects build orientation, positioning, and curing influence dimensional accuracy and flexural properties of stereolithographically printed resin. Dent Mater 2018;34:324–33. https://doi.org/10.1016/j.dental.2018.09.011.
[45] Li Haiyan, Wang Rongguo, Hu Honglin, Liu Wenbo. Surface modification of poly (urea-formaldehyde) microcapsules and the effect on the epoxy composites performance. J Macromol Sci Part A 2010;47:991–5. https://doi.org/10.1016/j.apsusc.2008.06.170.
[46] Cai XL, Fu DT, Qu AL. Effects of surface modification on the properties of microcapsules for self-healing. J Wuhan Univ Technol Mater Sci 2015;30:1234–9. https://doi.org/10.1179/1743289814Y.0000000081.
[47] Hamza TA, Rosenstiel SF, Elhosary MM, Ibraheem RM. The effect of fiber reinforcement on the fracture toughness and flexural strength of provisional restorative resins. J Prosthet Dent 2004;91:258–64. https://doi.org/10.1016/j.prosdent.2004.01.005.
[48] Brown EN, White SR, Sottos NR. Microcapsule induced toughening in a self-healing polymer composite. J Mater Sci 2004;39:1703–10. https://doi.org/10.1023/B:JMSC.0000016173.73733.dc.
[49] Henghua Jin Gina M, Miller Nancy R, Sottos, Scott RWhite. Fracture and fatigue response of a self-healing epoxy adhesive. Polym 2011;52:1628–34. https://doi.org/10.1016/j.polymer.2011.02.011.
[50] Philipp Michael Diana Döhler, Wolfgang HBinder. Improving autonomous self healing via combined chemical/physical principles. Adv Funct Mater 2008;18:44–52. https://doi.org/10.1016/j.polymer.2015.01.041.
[51] Ravandi R, Zeinali Heris S, Hemmati S, Davaran S. Development of a novel self-healing dental nanocomposite containing PUF nanocapsules and nanoclay. Mater Today Chem 2023;27:101302. https://doi.org/10.1016/j.mtchem.2022.101302.
[52] Alhotan A, Yates J, Zidan S, Haider J, Silikas N. Assessing fracture toughness and impact strength of PMMA reinforced with nano-particles and fibre as advanced denture base materials. Mater (Basel 2021;14:4127. https://doi.org/10.3390/ma14154127.
[53] Evans AG. The strength of brittle materials containing second phase dispersions. Philos Mag 1972;26:1327–44. https://doi.org/10.1080/14786437208220346.
[54] Wu J, Weir MD, Melo MA, Strassler HE, Xu HH. Effects of water-aging on self-healing dental composite containing microcapsules. J Dent 2016;47:86–93. https://doi.org/10.1016/j.jdent.2016.01.008.
[55] Wu J, Xie X, Zhou H, Tay FR, Weir MD, Melo MA, et al. Development of a new class of self-healing and therapeutic dental resins. Polym Degrad Stabi 2019;163:87–99. https://doi.org/10.1016/j.polymdegradstab.2019.02.024.
[56] Al-Dwairi ZN, Al Haj Ebrahim AA, Baba NZ. A comparison of the surface and mechanical properties of 3D printable denture-base resin material and conventional polymethylmethacrylate (PMMA). J Prosthodont 2023;32:40–8. https://doi.org/10.1111/jopr.13491.
[57] Aati S, Akram Z, Shrestha B, Patel J, Shih B, Shearston K, et al. Effect of post-curing light exposure time on the physico-mechanical properties and cytotoxicity of 3D-printed denture base material. Dent Mater 2022;38:57–67. https://doi.org/10.1016/j.dental.2021.10.011.
[58] Tanaka K, Taira M, Shintani H, Wakasa K, Yamaki M. Residual monomers (TEGDMA and Bis-GMA) of a set visible-light-cured dental composite resin when immersed in water. J Oral Rehabil 1991;18:353–62. https://doi.org/10.1111/j.1365-2842.1991.tb00067.x.